IEEE Photonics Journal
An IEEE Photonics Society Publication

Photonic Generation of Ultrawideband Signals With Large Carrier Frequency Tunability Based on an Optical Carrier Phase-Shifting Method

Volume 5, Number 5, October 2013

Wei Li
Li Xian Wang
Jian Yu Zheng
Ming Li, Member, IEEE
Ning Hua Zhu, Member, IEEE

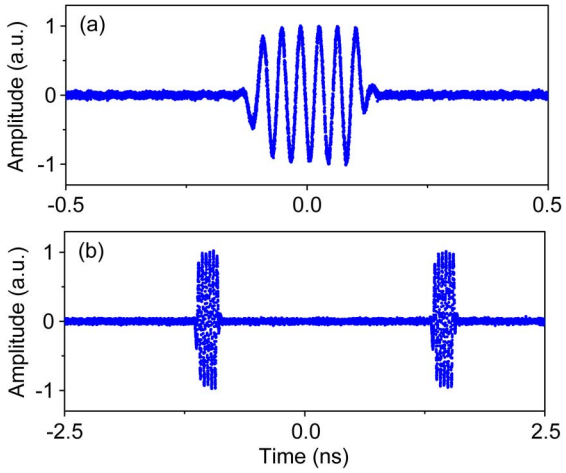

DOI: 10.1109/JPHOT.2013.2284260
1943-0655 © 2013 IEEE

Photonic Generation of Ultrawideband Signals With Large Carrier Frequency Tunability Based on an Optical Carrier Phase-Shifting Method

Wei Li, Li Xian Wang, Jian Yu Zheng, Ming Li, *Member, IEEE*, and Ning Hua Zhu, *Member, IEEE*

State Key Laboratory on Integrated Optoelectronics, Institute of Semiconductors, Chinese Academy of Sciences, Beijing 100083, China

DOI: 10.1109/JPHOT.2013.2284260

Manuscript received July 16, 2013; revised September 23, 2013; accepted September 23, 2013. Date of publication October 2, 2013; date of current version October 8, 2013. This work was supported by the National Natural Science Foundation of China under Grants 61377069, 61108002, 61090390, and 61275078. Corresponding author: N. H. Zhu (e-mail: nhzhu@semi.ac.cn).

Abstract: We theoretically and experimentally demonstrated a novel photonic approach to generating ultrawideband (UWB) pulses with large carrier frequency tunability based on an optical carrier phase-shifting technique by cascading polarization modulators (PolMs) and a polarizer. The UWB pulses are generated by truncating a continuous wave (CW) RF signal into a pulsed signal in a photodetector (PD). The experimental results show that the base-band frequency components and the strong residual local oscillator (LO) signal are well suppressed. In addition, the generated UWB signals satisfy the Federal Communications Commission (FCC) spectral mask very well.

Index Terms: Ultrawideband (UWB), microwave photonics.

1. Introduction

Ultra-wideband (UWB) signal has been a hot topic over the past few years for wireless communications and sensor networks because of its many advantages, e.g., low power consumption, immunity to multipath fading, and low interference with other narrow bandwidth communications [1]–[3]. The Federal Communications Commission (FCC) has defined the UWB as a radio technique with bandwidth larger than 500 MHz or larger than 20% fractional bandwidth and power density lower than −41.3 dBm/MHz. Several frequency bands have been regulated for UWB applications, including the centimeter wave (CMW) band from 3.1 to 10.6 GHz for indoor communications and the millimeter wave (MMW) band between 22 and 29 GHz for outdoor communications [1]. To overcome the short propagation range of the UWB signals, which is generally limited by the extremely low power density, UWB-over-fiber systems have been proposed to increase the transmission range [2], [3]. Therefore, it is highly desirable to directly generate UWB signals in the optical domain [4]–[18]. We focus on the generation of UWB signals using photonic method in this work.

So far, photonic generation of UWB signals has been proposed based on various methods [4]–[17]. For CMW UWB generation, cross gain or cross phase modulation in semiconductor optical amplifier (SOA) [4], [5], phase-to-intensity modulation conversion [2], and four-wave mixing in highly nonlinear fiber have been exploited [6], [7]. These methods are equivalent to microwave photonic filters with positive and negative coefficients [8]. To fully satisfy the FCC mask, multi-tap microwave

photonic filters have to be implemented [8]–[10], which increases the complexity of the system. On the other hand, directly photonic frequency up-conversion has been considered as one of the promising solutions for MMW UWB signals generation [11]–[14]. The baseband UWB signals can be up-converted to the MMW band based on a fiber optical parametric amplifier [11], four-wave mixing effect [7], and a Mach-Zehnder modulator [12], [13]. It is noticed that the up-converted UWB signals have a strong residual local oscillator (LO) component due to the beating between two distinguished optical carriers [11]–[13]. This strong residual LO component will reduce the dynamic range of the receiver and violate the FCC spectral mask for noninterference operation with other wireless standards. Therefore, power attenuation has to be done to match the FCC spectral mask, which in turn sacrifices the spectral efficiency. In spite of the strong residual LO signal, the baseband UWB signals can also be detected in the photodetector (PD). The baseband frequency components are usually undesirable because they will interfere with other narrowband standards.

Several methods have been reported to suppress the strong residual LO signal and the baseband frequency components [14]–[18]. In [14], the strong residual LO signal was suppressed using an intensity modulation scheme with high extinction ratio. However, the baseband frequency components were still existed, which can be eliminated by time-domain "background-subtraction" method using a balanced PD [15]. Other techniques reported in [16]–[18] can suppress the strong residual LO signal and the baseband frequency components at the same time by means of optical frequency shift keying modulation [16] or optical switch [17], [18]. In [17] and [18], the UWB signals are generated by switching the optical signals between two states, one of which has only a pure optical carrier. The other state consists of both the optical carrier and the modulation sideband. However, the carrier frequency of the generated UWB signal is restricted by the bandwidth and the roll-off property of the optical bandpass filter used in [17]. Moreover, the scheme presented in [18] is highly sensitive to the environmental fluctuation due to the polarization splitting and combining in a Mach-Zehnder structure.

In this paper, we present a novel photonic signal mixing approach to generating UWB pulses with large carrier frequency tunability based on optical carrier phase-shifting technique by cascading polarization modulators (PolMs) and a polarizer. An optical carrier and two modulation sidebands with orthogonal polarization states are generated by the first PolM driven by a sinusoidal RF signal. The optical carrier phase-shift θ (i.e., the phase-shift between the optical carrier and the two sidebands) is controlled by the electrical driving signal of the second PolM. The polarizer is added to combine the optical carrier and the sidebands to a fixed linear polarization state. For $\theta = \pi/2$, the RF signal cannot be detected in the PD because the beat signals between the optical carrier and the sidebands cancel each other out perfectly. For $\theta \neq \pi/2$, the RF signal can be recovered in the PD. The power of the recovered RF signal reaches the maximum for $\theta = 0$ or π. As a result, the UWB signals can be generated by truncating the continuous wave (CW) RF signal into a pulsed one in the PD. The baseband frequency components are well suppressed because the optical power launched to the PD keeps constant all the time. Meanwhile, the strong residual LO signal is also suppressed since the CW RF signal is completely turned off for $\theta = \pi/2$. The carrier frequency of the generated UWB signal is widely tunable because there is no optical filter used in our scheme. The feasibility of the proposed scheme is theoretically analyzed and experimentally verified. The generated UWB pulses satisfy the FCC masks very well.

2. Principle

The schematic diagram of the proposed scheme is shown in Fig. 1(a), which consists of a laser diode (LD), two PolMs, a polarizer, two polarization controllers (PCs), and a PD. A sinusoidal RF signal with amplitude of V_{RF} and angular frequency of ω_{RF} is driven to the first PolM to produce an optical carrier and two sidebands. Mathematically, the optical field at the output of the PolM is given by [19]

$$\vec{E}_{\mathrm{PolM1}}(t) = \frac{1}{\sqrt{2}}\left[\hat{x}\cdot e^{j\omega_0 t + j\beta_1 \cos(\omega_{\mathrm{RF}} t)} + \hat{y}\cdot e^{j\omega_0 t - j\beta_1 \cos(\omega_{\mathrm{RF}} t)}\right] \quad (1)$$

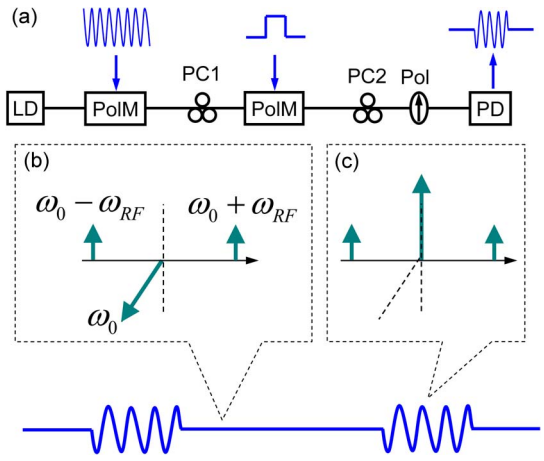

Fig. 1. (a) Experimental setup (LD: laser diode; PolM: polarization modulator; PC: polarization controller; Pol: polarizer; PD: photodetector). (b) and (c) The principal of the proposed UWB generation technique.

where ω_0 is the angular frequency of the optical carrier. β_1 is the phase modulation index of the first PolM, expressed in radians as $\beta_1 = \pi V_{\mathrm{RF}}/V_{\pi 1}$, and $V_{\pi 1}$ is the half-wave voltage of the first PolM. $\hat{x}$ and $\hat{y}$ are aligned with the two principal polarization axes of the first PolM, respectively. The phase difference between the two polarization states is ignored. Applying the Jacobi-Anger expansion to Eq. (1), we have

$$\vec{E}_{\mathrm{PolM1}}(t) = \frac{1}{\sqrt{2}} e^{j\omega_0 t}\left(\hat{x}\cdot\sum_{n=-\infty}^{n=\infty} j^n \cdot J_n(\beta_1) e^{jn\omega_{\mathrm{RF}}t} + \hat{y}\cdot\sum_{n=-\infty}^{n=\infty} j^n \cdot J_n(-\beta_1) e^{jn\omega_{\mathrm{RF}}t}\right) \tag{2}$$

where $J_n(\cdot)$ is the Bessel function of the first kind of order n. Considering the small-signal modulation condition, Eq. (2) can be simplified as

$$\vec{E}_{\mathrm{PolM1}}(t) = \frac{1}{\sqrt{2}} e^{j\omega_0 t}\cdot\left\{\hat{x}'\cdot\left[J_1(\beta_1)e^{j\omega_{\mathrm{RF}}t+j\pi/2} + J_1(\beta_1)e^{-j\omega_{\mathrm{RF}}t+j\pi/2}\right] + \hat{y}'\cdot J_0(\beta_1)\right\} \tag{3}$$

where the polarization axes of $\hat{x}'$ and $\hat{y}'$ are aligned with $\hat{x}+45^\circ$ and $\hat{y}+45^\circ$, respectively. The optical carrier and sidebands are polarized at 45° and -45° relative to the x axis of the first PolM, respectively [20]. The principal polarization axes of the second PolM are oriented at an angle of 45° to that of the first PolM via adjusting the PC1. It is known that the modulation indexes of the PolM are opposite for the TE and TM modes. Therefore, the optical carrier and sidebands experience different phase modulations. The optical field at the output of the second PolM can be expressed as

$$\vec{E}_{\mathrm{PolM2}}(t) = \frac{1}{\sqrt{2}} e^{j\omega_0 t}\cdot\left\{\hat{x}'\cdot\left[J_1(\beta_1)e^{j\omega_{\mathrm{RF}}t+j\pi/2} + J_1(\beta_1)e^{-j\omega_{\mathrm{RF}}t+j\pi/2}\right]e^{j\pi V(t)/V_{\pi 2}} + \hat{y}'\cdot J_0(\beta_1)e^{j\eta\pi V(t)/V_{\pi 2}}\right\} \tag{4}$$

where $V_{\pi 2}$ is the half-wave voltage of the second PolM, and η is the ratio of phase modulation efficiency for the TM polarization to the TE polarization. For the PolM, we have $\eta = -1$. $V(t)$ is the electrical signal applied to the second PolM. The polarizer oriented at an angle of 45° to one principal axis of the second PolM is used to combine the optical carrier and the sidebands to a fixed linear polarization state. The optical field at the output of the polarizer can be expressed as

$$\vec{E}_{\mathrm{pol}}(t) = \frac{1}{2} e^{j\omega_0 t}\left\{\left[J_1(\beta_1)e^{j\omega_{\mathrm{RF}}t+j\pi/2} + J_1(\beta_1)e^{-j\omega_{\mathrm{RF}}t+j\pi/2}\right]e^{j\pi V(t)/V_{\pi 2}} + J_0(\beta_1)e^{j\eta\pi V(t)/V_{\pi 2}}\right\}. \tag{5}$$

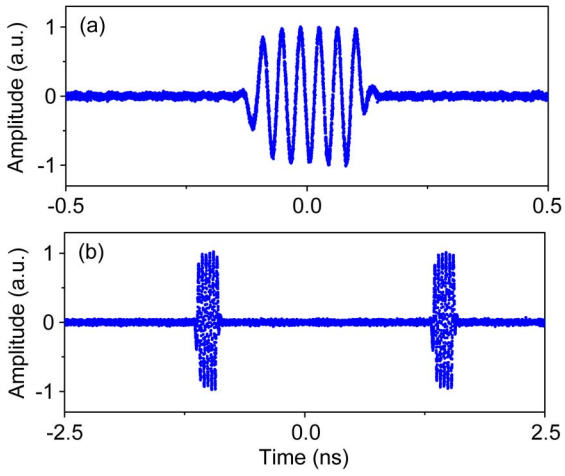

Fig. 2. (a) Measured MMW UWB pulse at the RF carrier frequency of 26 GHz. (b) Measured MMW UWB pulses in a larger time scale of 5 ns.

After the polarizer, the optical signal is detected in the PD. The photocurrent is given by

$$i(t) \propto E_{\text{pol}}(t) \cdot E_{\text{pol}}^{*}(t) \approx \frac{1}{4} J_0^2(\beta_1) + \frac{1}{2} J_1^2(\beta_1) - J_0(\beta_1) J_1(\beta_1) \cdot \sin\left[\frac{(1-\eta)\pi V(t)}{V_{\pi 2}}\right] \cdot \cos(\omega_{\text{RF}} t). \quad (6)$$

The photocurrent consists of ac and dc parts. A sinusoidal RF signal at the frequency of ω_{RF} is recovered, whose amplitude is determined by a sine term. For $V(t) = 0$, the RF signal cannot be detected in the PD, as shown in Fig. 1(b). It can be expected that the strong residual LO signal could be well suppressed since the CW RF signal is completely turned off when $V(t)$ equals to 0. For $V(t) \neq 0$, the RF signal can be detected in the PD, as shown in Fig. 1(c). In this way, UWB signals can be generated by truncating the CW RF signal into a pulsed RF signal. For $V(t) > 0$ or < 0, the phase of the recovered microwave signal will be 0 and π, respectively. Therefore, the proposed method can also be used to generate binary phase-coded microwave signal, which has been demonstrated elsewhere [19]. On the other hand, the dc part of Eq. (6) is independent of the electrical signals applied to the second PolM, which means that the baseband frequency components are eliminated because the total optical power launched to the PD keeps constant all the time.

3. Experiments and Results

Experimental verification of the proposed scheme was carried out based on the experimental setup shown in Fig. 1(a). The second PolM shown in Fig. 1(a) was replaced by a phase modulator (PM) because we have only one PolM in our laboratory. It is noted that we have $\eta \approx 1/3$ [19] for the ithium-niobate PM rather than $\eta = -1$ for the PolM. The principal polarization axes of the PolM, the PM, and the polarizer were set as described in Section 2 by adjusting the PCs. A linearly polarized optical carrier from an LD emitting at a wavelength of 1550 nm was fiber-coupled to the PolM. A polarizer is integrated at the input of the PolM with an angle of 45° to one principal axis of the PolM. A sinusoidal LO signal from an electrical signal generator (ESG) was fed to the PolM. The PM was driven by a rectangular signal from a pulse pattern generator (PPG). The PPG was custom-defined as a 32-bit fixed pattern "1110 0000 ... 0000" (three "1" every 32 bits).

First of all, the proposed system was tested for MMW UWB signal generation. To this end, the sinusoidal LO signal from the ESG was set at a frequency of 26 GHz to match the FCC spectral mask. The PPG was triggered by the LO signal from the ESG after a 1/2 frequency divider. Therefore, the PPG operated at a speed of 13 Gb/s with the peak-to-peak amplitude of 1 V. This is equivalent to a pulse train with a repetition rate of ~400 MHz and a duty cycle of 3/32. Fig. 2(a)

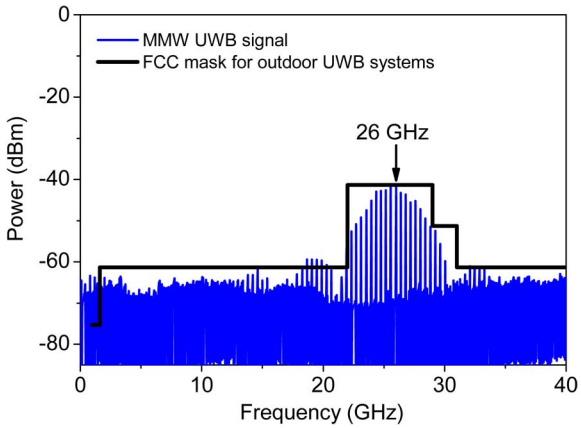

Fig. 3. Measured electrical spectrum of the generated MMW UWB signals at the RF carrier frequency of 26 GHz.

shows the measured MMW UWB pulse at the RF carrier frequency of 26 GHz, which was captured by a sampling oscilloscope. To clearly show the MMW UWB pulses, the generated signals were measured in a larger time scale of 5 ns, as shown in Fig. 2(b). The duty cycle of the pulse train is 3/32 as expected. It is apparent that the CW RF signal was truncated into RF pulses with pulse duration of 0.23 ns. It can be expected that the baseband frequency components of the generated UWB pulses could be eliminated in the electrical domain since there is no pedestal in the time-domain pulse.

Fig. 3 shows the electrical spectrum of the generated MMW UWB signal, which was measured by an electrical spectrum analyzer (ESA). The electrical spectrum is centered at the frequency of 26 GHz with a frequency interval of $\sim$400 MHz between the adjacent frequency components as expected. The electrical spectrum consists of a mainlobe and a series of sidelobes, which can be attributed to the Fourier transform of the rectangular envelope of the RF pulses. It is worth noting that the undesirable baseband frequency components and the strong residual LO signal are well suppressed. The FCC spectral mask for outdoor UWB systems is also shown in Fig. 3. It can be seen that the electrical spectrum satisfies the FCC mask very well.

To show the RF carrier frequency tunability of the proposed system, CMW UWB signal was also generated by tuning the LO signal coming from the ESG to a frequency of 7 GHz. To fully fill the FCC mask for indoor communications, the PPG still operated at the speed of 13 Gb/s. This time, however, the PPG cannot be triggered by the RF signal (7 GHz) from the ESG. As a result, we cannot measure the UWB pulse in the time domain since the sampling oscilloscope cannot be synchronously triggered either. In this context, the electrical spectrum of the generated CMW UWB signal was measured, as shown in Fig. 4. The electrical spectrum is centered at 7 GHz with a frequency interval of $\sim$400 MHz between the adjacent frequency components. In order to clearly show the difference between the suppressed baseband frequency components and the sidelobe of the generated UWB signal, the suppressed baseband frequency components is drawn in red line in the frequency range from dc to $\sim$2 GHz. It can be seen that the baseband frequency components are well suppressed. The FCC spectral mask for indoor UWB systems is also shown in Fig. 4. The generated CMM UWB spectrum satisfies the FCC mask very well except for the dip from 0.96 to 1.61 GHz. The dip was contaminated by the frequency components of the sidelobe. The envelope of the generated electrical spectrum shown in Fig. 4 is a sinc function, which is the Fourier transform of the rectangle pulse. The sidelobes could be eliminated if an electrical Gaussian pulse is applied to the PM instead of the rectangular pulse. It is worth noting that, for the proposed method, the carrier frequency can be tunable in a large frequency range which is only limited by the bandwidth of the devices used in our experiment. The long-term stability of the proposed system may be affected by the stability of the PolM, PM, PCs, and polarizer. However, the stability of the

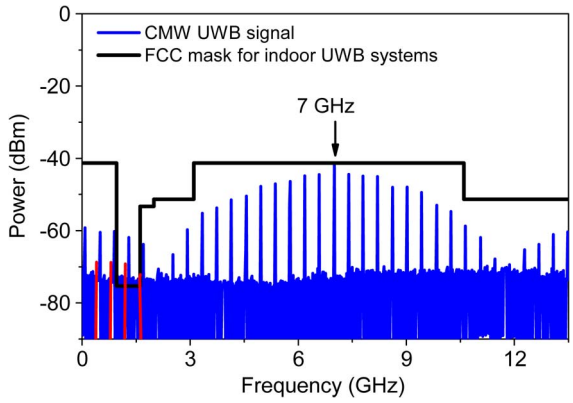

Fig. 4. Measured electrical spectrum of the generated CMW UWB signals at the RF carrier frequency of 7 GHz.

system can be improved if polarization maintaining fibers are used instead of PCs. Moreover, the stability of the system can be further improved if the PolM, the PM, and the polarizer are integrated on one chip.

4. Conclusion

We have theoretically and experimentally demonstrated a photonic approach to generating UWB pulses with large carrier frequency tunability based on an optical carrier phase-shifting method by cascading PolMs (or PM) and a polarizer. The UWB signals were generated by truncating the CW RF signal into the pulsed RF signal in the PD. The baseband frequency components and the strong residual LO signal were well suppressed. The carrier frequency tunable UWB signals were experimentally generated in the CMW band at the carrier frequency of 7 GHz and in the MMW band at the carrier frequency of 26 GHz. In addition, the experimental results show that the generated UWB pulses are well FCC-compliant.

References

[1] G. R. Aiello and G. D. Rogerson, "Ultra-wideband wireless systems," *IEEE Microw. Mag.*, vol. 4, no. 2, pp. 36–47, Jun. 2003.
[2] J. Yao, F. Zeng, and Q. Wang, "Photonic generation of ultrawideband signals," *J. Lightw. Technol.*, vol. 25, no. 11, pp. 3219–3235, Nov. 2007.
[3] S. Pan and J. P. Yao, "UWB over fiber communications: Modulation and transmission," *J. Lightw. Technol.*, vol. 28, no. 16, pp. 2445–2455, Aug. 2010.
[4] Q. Wang, F. Zeng, S. Blais, and J. Yao, "Optical ultrawideband monocycle pulse generation based on cross-gain modulation in a semiconductor optical amplifier," *Opt. Lett.*, vol. 31, no. 21, pp. 3083–3085, Nov. 2006.
[5] J. Dong, X. Zhang, J. Xu, D. Huang, S. Fu, and P. Shum, "Ultrawideband monocycle generation using cross-phase modulation in a semiconductor optical amplifier," *Opt. Lett.*, vol. 32, no. 10, pp. 1223–1225, May 2007.
[6] W. Li, L. X. Wang, W. Hofmann, N. H. Zhu, and D. Bimberg, "Generation of ultra-wideband triplet pulses based on four-wave mixing and phase-to-intensity modulation conversion," *Opt. Exp.*, vol. 20, no. 18, pp. 20 222–20 227, Aug. 2012.
[7] F. Zhang, J. Wu, S. Fu, K. Xu, Y. Li, X. Hong, P. Shum, and J. Lin, "Simultaneous multi-channel CMW-band and MMW-band UWB monocycle pulse generation using FWM effect in a highly nonlinear photonic crystal fiber," *Opt. Exp.*, vol. 18, no. 15, pp. 15 870–15 875, Jul. 2010.
[8] M. Bolea, J. Mora, B. Ortega, and J. Capmany, "Optical UWB pulse generator using an*N* tap microwave photonic filter and phase inversion adaptable to different pulse modulation formats," *Opt. Exp.*, vol. 17, no. 7, pp. 5023–5032, Mar. 2009.
[9] E. Zhou, X. Xu, K.-S. Lui, and K. K.-Y. Wong, "A power-efficient ultra-wideband pulse generator based on multiple PM-IM conversions," *IEEE Photon. Technol. Lett.*, vol. 22, no. 14, pp. 1063–1065, Jul. 2010.
[10] S. T. Abraha, C. M. Okonkwo, E. Tangdiongga, and A. M. J. Koonen, "Power-efficient impulse radio ultrawideband pulse generator based on the linear sum of modified doublet pulses," *Opt. Lett.*, vol. 36, no. 12, pp. 2363–2365, Jun. 2011.
[11] J. Li, Y. Liang, and K. K. Y. Wong, "Millimeter-wave UWB signal generation via frequency up-conversion using fiber optical parametric amplifier," *IEEE Photon. Technol. Lett.*, vol. 21, no. 17, pp. 1172–1174, Sep. 2009.

[12] Y. L. Guennec and R. Gary, "Optical frequency conversion for millimeter-wave ultra-wideband-over fiber systems," *IEEE Photon. Technol. Lett.*, vol. 19, no. 13, pp. 996–998, Jul. 2007.
[13] Q. Chang, Y. Tian, T. Ye, J. Gao, and Y. Su, "A 24-GHz ultra-wideband over fiber system using photonic generation and frequency up-conversion," *IEEE Photon. Technol. Lett.*, vol. 20, no. 19, pp. 1651–1653, Oct. 2008.
[14] T. Kuri, Y. Omiya, T. Kawanishi, S. Hara, and K. Kitayama, "Optical transmitter and receiver of 24-GHz ultra-wideband signal by direct photonic conversion techniques," in *Proc. Int. Topical Meet. Microw. Photon.*, Grenoble, France, Oct. 2006, pp. 1–4.
[15] M. Abtahi, M. Dastmalchi, S. LaRochelle, and L. A. Rusch, "Generation of arbitrary UWB waveforms by spectral pulse shaping and thermally-apodized FBGs," *J. Lightw. Technol.*, vol. 27, no. 23, pp. 5276–5283, Dec. 2009.
[16] T. Kawanishi, T. Sakamoto, and M. Izutsu, "Ultrawide-band radio signal generation using optical frequency-shift-keying technique," *IEEE Microw. Wireless Compon. Lett.*, vol. 15, no. 3, pp. 153–155, Mar. 2005.
[17] L. X. Wang, W. Li, J. Y. Zheng, H. Wang, J. G. Liu, and N. H. Zhu, "High-speed microwave photonic switch for millimeter-wave ultra-wideband signal generation," *Opt. Lett.*, vol. 38, no. 4, pp. 579–581, Feb. 2013.
[18] Y. Du, J. Zheng, L. Wang, H. Wang, N. Zhu, and J. Liu, "Widely-tunable and background-free ultra-wideband signals generation utilizing polarization modulation-based optical switch," *IEEE Photon. Technol. Lett.*, vol. 25, no. 4, pp. 335–337, Feb. 2013.
[19] W. Li, L. X. Wang, M. Li, and N. H. Zhu, "Photonic generation of widely tunable and background-free binary phase-coded radio-frequency pulses," *Opt. Lett.*, vol. 38, no. 17, pp. 3441–3444, Sep. 2013.
[20] A. L. Campillo, "Orthogonally polarized single sideband modulator," *Opt. Lett.*, vol. 32, no. 21, pp. 3152–3154, Oct. 2007.